JOURNAL OF MATERIALS SCIENCE 29 (1994) 2147–2151

Melting behaviour of cadmium particles embedded in an aluminium matrix

D.L. ZHANG*, J. L. HUTCHINSON, B. CANTOR
Oxford Centre for Advanced Materials and Composites, Department of Materials, University of Oxford, Parks Road, Oxford OX1 3PH, UK

An Al–4.5% Cd alloy has been manufactured by melt spinning to produce a microstructure of 14–150 nm diameter faceted cadmium particles embedded in an aluminium matrix. The melting behaviour of the cadmium particles has been investigated by differential scanning calorimetry. The melting point of 20 and 14 nm diameter cadmium particles embedded are depressed by 7 and 9 K respectively, below the bulk equilibrium cadmium melting point, because of Gibbs–Thomson capillarity effects. The average solid cadmium particle/aluminium matrix interfacial energy is 27 mJ m^{-2} higher than the average liquid cadmium particle/aluminium matrix interfacial energy. No significant superheating is needed to nucleate cadmium particle melting.

1. Introduction

The melting point of small crystalline solid particles can differ from the bulk equilibrium melting point of the same material for several reasons: (1) Gibbs–Thomson capillarity effects; (2) pressure effects caused by differential thermal contraction between the particles and a surrounding solid matrix; (3) pressure effects caused by solidification shrinkage during solidification of the particles; and (4) kinetic barriers to the nucleation of particle melting. Many researchers have investigated the melting behaviour of small particles [1–16]. In general, for solid particles surrounded by their own vapour, the melting temperature is depressed below the bulk equilibrium melting point by an amount which is inversely proportional to the particle size [6–11]. However, for solid particles embedded in a high melting point solid matrix, the melting temperature can be either lower or higher than the bulk equilibrium melting point, and can either decrease or increase with decreasing particle size [12–16]. The present paper describes the results of an investigation into the melting behaviour of cadmium particles embedded in an aluminium matrix by a combination of transmission electron microscopy (TEM) and differential scanning calorimetry (DSC).

2. Experimental procedure

A hypomonotectic Al–4.5 wt % Cd alloy was manufactured by induction melting 99.999% pure aluminium and cadmium in a recrystallized alumina crucible under a dynamic argon atmosphere. Specimens of the resulting alloy ingot were then rapidly solidified by melt spinning. Alloy charges of 3–5 g were induction remelted in quartz crucibles under a dynamic argon atmosphere, held for 100 s at 800 °C and then ejected with an overpressure of 20 kPa through a 1 mm diameter orifice on to the outer surface of a polished copper wheel rotating with a tangential surface speed of either 12.5 or 33.5 m s^{-1}. The ribbon compositions were examined in a Cameca Camebax electron microprobe analyser and determined to be 4.47 wt % Cd.

Melt-spun Al–4.5 wt % Cd specimens were jet-electropolished in a mixture of 25 vol % nitric acid and 75 vol % methanol at −40 °C for metallographic examination in a Philips CM12 TEM and a Jeol 4000EX high-resolution TEM (HREM). The melting behaviour of cadmium particles in the melt-spun microstructure was investigated by heating and cooling experiments in a DuPont 1090 thermal analyser fitted with 910 DSC module. Individual samples of 15–20 mg were sealed in aluminium cans, heated at a rate of 10 K min^{-1} from 200 °C to a temperature in the range 312–350 °C, held for 600 s, and then cooled at a rate of 5 K min^{-1} to 200 °C, all under a dynamic argon atmosphere. Heat-flow differences between the sample and a similarly heat-treated reference were continuously recorded on a microcomputer for subsequent examination.

3. Results

Fig. 1a and b show typical transmission electron micrographs of the microstructure of Al–4.5 wt % Cd melt spun at 12.5 and 33.5 m s^{-1}, respectively. For both wheel speeds, the microstructure consisted of small cadmium particles homogeneously distributed throughout a matrix of aluminium. The cadmium particle diameters were in the range 20–150 nm at 12.5 m s^{-1}, and 14–120 nm at 33.5 m s^{-1}, i.e. the average cadmium particle size decreased with increasing wheel speed. The hcp cadmium particles were found to have an orientation relationship with the fcc aluminium matrix which can be described as: $\{1\,1\,1\}_{Al} \| \{0\,0\,0\,1\}_{Cd}$ and $\langle 1\,1\,0\rangle_{Al} \| \langle 1\,1\,\bar{2}\,0\rangle_{Cd}$, as

* *Present address*: Department of Materials Science and Engineering, Carnegie Mellon University, Pittsburgh, PA 15213, USA.

0022–2461

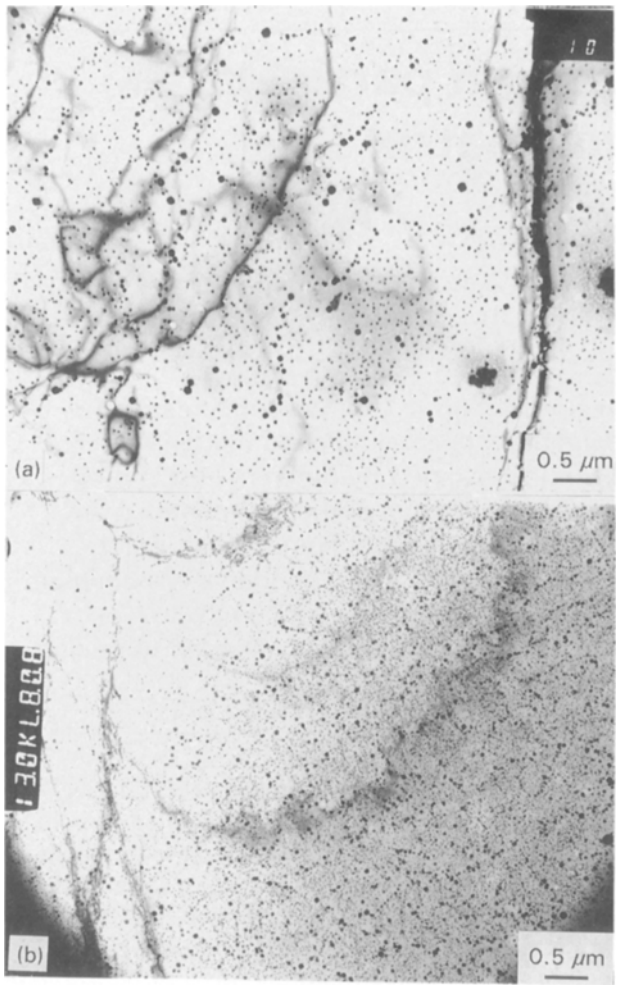

Figure 1 Transmission electron micrographs of the microstructure of Al–4.5 wt % Cd melt spun at wheel speeds of (a) 12.5 m s^{-1} and (b) 33.5 m s^{-1}.

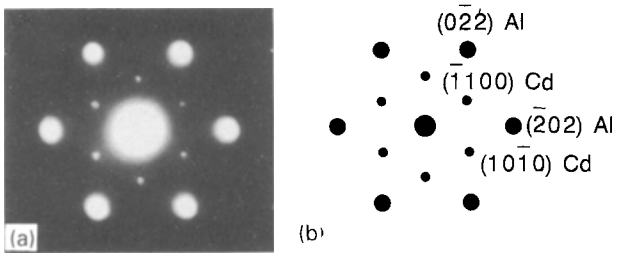

Figure 2 (a) Selected-area electron diffraction pattern from melt-spun Al–4.5 wt % Cd, showing superimposed $[1\,1\,1]_{Al}$ and $[0\,0\,0\,1]_{Cd}$ zones from the aluminium matrix and cadmium particles, respectively; (b) schematic electron diffraction pattern corresponding to (a).

shown by selected-area electron diffraction patterns such as in Fig. 2. The cadmium particles within the aluminium matrix grains were surrounded by two $\{1\,1\,1\}_{Al}\|\{0\,0\,0\,1\}_{Cd}$ facets separated by curved interface regions, as shown by the HREM micrograph in Fig. 3. Ledges were sometimes present on the $\{1\,1\,1\}_{Al}\|\{0\,0\,0\,1\}_{Cd}$ facets as shown in Fig. 3. The cadmium particle/aluminium matrix orientation relationship and the cadmium particle faceting behaviour have been discussed in more detail elsewhere [17].

Fig. 4a and b show typical DSC traces of cadmium particle melting endotherms from Al–4.5 wt % Cd melt spun at 12.5 and 33.5 m s^{-1}, respectively. The

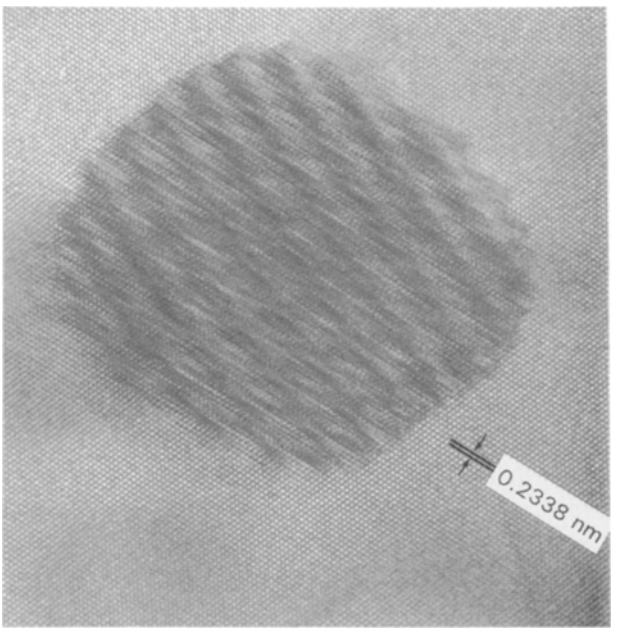

Figure 3 HREM from melt-spun Al–4.5 wt % Cd, showing cadmium particle shape with electron beam parallel to a $\langle 1\,1\,0\rangle_{Al}$ zone axis.

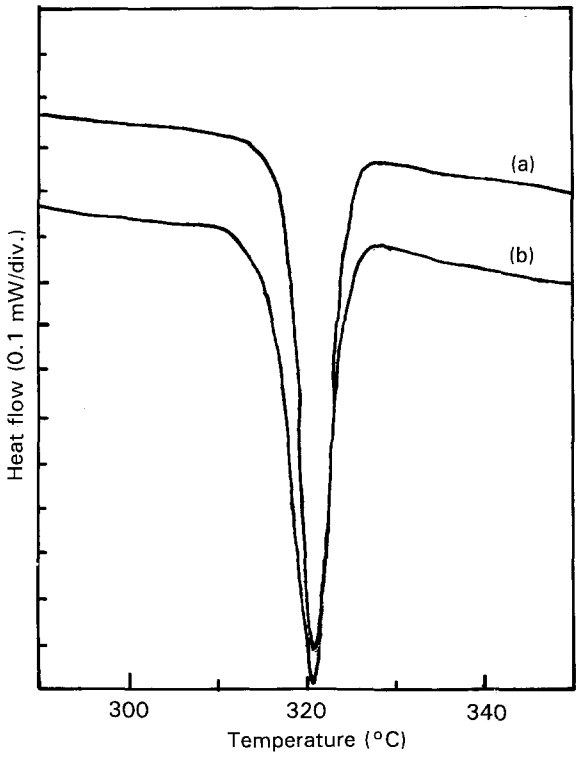

Figure 4 DSC traces of cadmium particle melting endotherms from Al–4.5 wt % Cd melt spun at wheel speeds of (a) 12.5 m s^{-1} and (b) 33.5 m s^{-1}.

cadmium particles always melted with a single sharp endothermic peak, with onset temperatures of 314 and 312 °C for wheel speeds of 12.5 and 33.5 m s^{-1}, respectively, i.e. the onset temperature of cadmium particle melting decreased slightly with increasing wheel speed. Fig. 5a shows the volume fraction of molten cadmium particles as a function of temperature for Al–4.5 wt % Cd melt spun at 33.5 m s^{-1}, determined by heating a series of specimens in the DSC to different annealing temperatures in the range 310–350 °C,

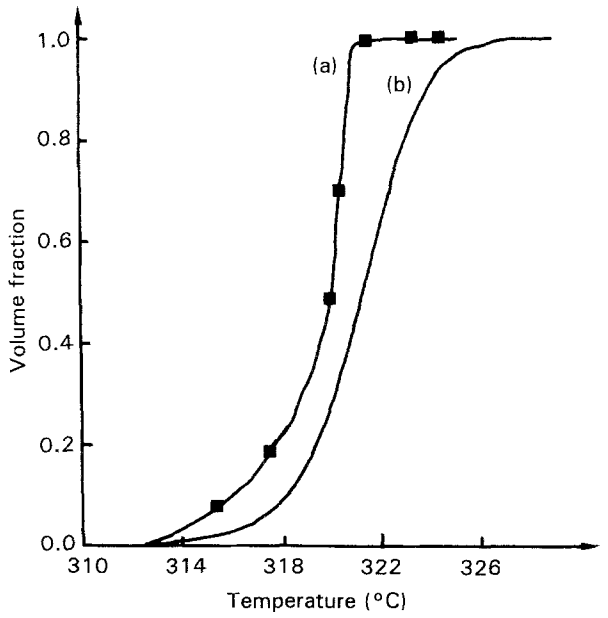

Figure 5 Volume fraction of molten cadmium particles from Al–4.5 wt % Cd melt spun at 33.5 m s^{-1} as a function of temperature determined by (a) heating in the DSC to different temperatures within the melting range and then cooling to measure the solidification heat for each annealing temperature, and (b) integrating the cadmium particle melting endotherm.

i.e. in the range of cadmium particle melting temperature, followed by holding for 600 s, and then cooling to measure the solidification heat for each annealing temperature. From Fig. 5a for 600 s anneals, all the cadmium particles melted when melt-spun Al–4.5 wt % Cd was heated to the bulk equilibrium cadmium melting point of 321 °C [18]. Approximately 70% of the cadmium particles melted within 2.5 K of 321 °C, and the remaining 30% melted at temperatures 2.5–9 K below 321 °C. Fig. 5b also shows the volume fraction of molten cadmium particles as a function of temperature for Al–4.5 wt% Cd melt spun at 33.5 m s^{-1}, determined by integrating cadmium particle melting endotherms such as shown in Fig. 4b. From Fig. 5b for continuous heating, approximately 75% of the cadmium particles melted at temperatures within 2.5 K of 321 °C, approximately 12.5% melted at temperatures 2.5–9 K below 321 °C, and approximately 12.5% melted 2.5–4 K above 321 °C. For any given volume fraction of melted cadmium particles, Fig. 5b extended to 1–3 K higher temperatures than Fig. 5a.

Fig. 6a–c show typical DSC traces of cadmium particle solidification exotherms from Al–4.5 wt % Cd melt spun at 33.5 m s^{-1}, as a function of annealing temperature in the range 312–350 °C, i.e. in the range of cadmium particle melting temperature. The cadmium particles always solidified with a single sharp exothermic peak. The onset, peak and end temperatures of the cadmium particle solidification exotherm were independent of annealing temperature within the range of cadmium particle melting, but the size of the solidification exotherm increased with increasing annealing temperature as more of the cadmium particles melted. The cadmium particle solidification behaviour has been discussed in more detail elsewhere [17, 19].

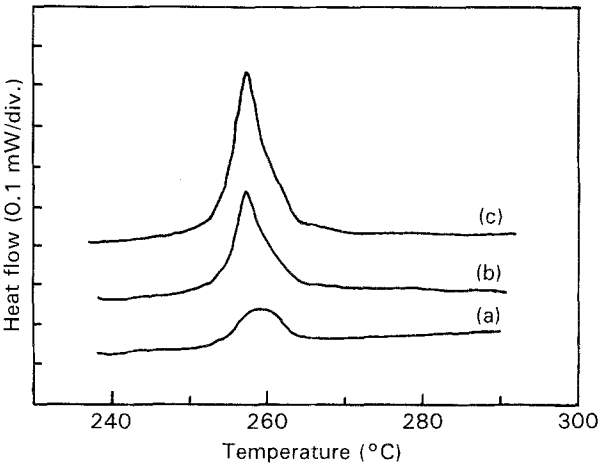

Figure 6 DSC traces of cadmium particle solidification exotherms from Al–4.5 wt % Cd melt spun at 33.5 m s^{-1} as a function of annealing temperature in the range of cadmium particle melting: (a) 317.4 °C, (b) 319.9 °C, and (c) 321.3 °C.

4. Discussion

Fig. 5a and b show the volume fraction of molten cadmium particles as a function of temperature for 600 s anneals and continuous heating, respectively. For a given volume fraction of molten cadmium particles, Fig. 5b extends to 1–3 K higher temperatures than Fig. 5a. There are three possible reasons for this difference:

(1) instrumental thermal lag during continuous heating. However, the DSC is accurately calibrated for continuous heating, with the melting onset temperature independent of heating rate within the experimental error of $\pm$ 0.1 K. In other words, the thermal lag must be less than $\pm$ 0.1 K, much smaller than the observed temperature difference between Fig. 5a and b.

(2) kinetic delay for growth of the cadmium melts after nucleation of cadmium particle melting. For a cadmium particle diameter of 120 nm at a heating rate of 10 K min^{-1}, the observed temperature difference of 3 K between Fig. 5a and b corresponds to a melting time of 18 s, and a melting growth velocity of about 7 nm s^{-1}. This is unreasonably low for melting by many orders of magnitude, indicating that growth kinetics are insignificant compared with the observed temperature difference between Fig. 5a and b.

(3) kinetic delay for nucleation of cadmium particle melting. For a heating rate of 10 K min^{-1}, the observed temperature difference of 3 K between Fig. 5a and b corresponds to a time of 18 s to nucleate melting in all the cadmium particles of a given size. This is not unreasonable, because of the very small size and therefore very large number of cadmium particles in each DSC specimen. In addition, previous *in situ* experiments in the TEM have shown directly than indium and lead particles embedded in an aluminium matrix melt at different times over a range of 10–20 s [16]. In summary, the temperature difference between Fig. 5a and b is caused by the kinetic delay in nucleating melting in a very large number of small cadmium particles.

The cadmium particle melting endotherms on the DSC traces are very similar for the two melt-spinning

wheel speeds of 12.5 and 33.5 m s^{-1}, with most of the cadmium particles melting at temperatures very close to the bulk equilibrium cadmium melting point of 312 °C. However, there are low-temperature tails on the cadmium particle melting endotherms which extend 7 and 9 K below 312 °C for wheel speeds of 12.5 and 33.5 m s^{-1}, respectively. In other words, some of the cadmium particles melt at lower temperature when the melt-spinning wheel speed is increased, and this correlates with a decrease in the cadmium particle size, as shown in Fig. 1. The maximum depression of cadmium melting point is 7 K corresponding to the smallest cadmium particle diameter of 20 nm at 12.5 m s^{-1}, and 9 K corresponding to the smallest cadmium particle diameter of 14 nm at 33.5 m s^{-1}. This depression of cadmium melting point may be caused by pressure effects associated with either differential thermal contraction, solidification shrinkage, or Gibbs–Thomson capillarity.

The combined effects of differential thermal contraction and solidification shrinkage on the cadmium particle melting point in melt-spun Al–4.5 wt % Cd can be estimated as follows

$$\Delta T_1 = (V_L K_L + (V_S - s) K_S) T_m / L_V \quad (1)$$

where ΔT is the change in cadmium melting point from the bulk equilibrium melting point T_m, K_L and K_S are the bulk moduli of liquid and solid cadmium, respectively, V_L and V_S are the fractional volume changes associated with differential thermal contraction of the liquid and solid cadmium particles, respectively, $-s$ is the solidification shrinkage, and L_V is the latent heat of melting per unit volume of cadmium. V_L and V_S can be calculated from

$$V_L = 3(T_{mo} - T_m)(a_{Al} - a_{LCd}) \quad (2)$$

$$V_S = 3(T_m - T_R)(a_{Al} - a_{SCd}) \quad (3)$$

where T_{mo} and T_R are the monotectic temperature and room temperature, respectively, and a_{Al}, a_{LCd} and a_{SCd} are the linear coefficients of thermal expansion of solid aluminium, liquid cadmium and solid cadmium, respectively. In the absence of cavitation, fracture or flow to relieve differential thermal contraction and solidification shrinkage stresses, Equation 1 predicts that the change in equilibrium melting point, ΔT_1, is independent of particle size, and positive or negative depending on the relative magnitudes of the different terms in Equation 1. Taking $K_L = K_S = 55$ GPa, $s = 0.047$, $a_{LCd} = a_{SCd} = 31.3$ μm m^{-1} K^{-1}, $a_{Al} = 27.4$ μm m^{-1} K^{-1}, $L_V = 475.3$ MJ m^{-3}, $T_m = 594$ K, $T_R = 298$ K and $T_{mo} = 923$ K (19, 20), Equations 1–3 give $\Delta T = -3733$ K. The measured melting point depression is three orders of magnitude smaller, and increases with decreasing particle size. In other words, the differential thermal contraction and solidification shrinkage stresses must be relieved by cavitation, fracture or flow, removing any significant influence on the cadmium particle melting point.

The cadmium particles in melt-spun Al–4.5 wt % Cd are also subject to hydrostatic stress caused by Gibbs–Thomson capillarity forces from the curvature of the particle surfaces. The hydrostatic capillarity stresses are associated with changes in chemical potential which are different for the solid and liquid cadmium particles. The effect of Gibbs–Thomson capillarity on cadmium particle melting point in melt-spun Al–4.5 wt % Cd can be estimated as follows

$$\Delta T_2 = 2(\sigma_L/\rho_L - \sigma_S/\rho_S) T_m \rho_L / L_V r \quad (4)$$

where ΔT_2 is the change in cadmium particle melting point from the bulk equilibrium melting point, ρ_L and ρ_S are the densities of liquid and solid cadmium, respectively, and σ_L and σ_S are the solid aluminium–liquid cadmium and solid aluminium–solid cadmium surface energies, respectively, averaged over all of the cadmium particle surfaces including contributions from the flat facets and curved regions as shown in Fig. 3. Equation 4 predicts that the change in cadmium melting point, ΔT_2, is inversely proportional to particle size and positive or negative depending on the relative magnitude of the two terms in Equation 4. This prediction is in good agreement with the DSC results. Taking $\Delta T_2 = 7$ and 9 K corresponding to $r = 10$ and 7 nm, respectively, $T_m = 594$ K, $\rho_L = \rho_S = 8.33$ Mg m^{-3} and $L_V = 475.3$ MJ m^{-3} [18, 20], Equation 4 gives the difference in average solid aluminium–solid cadmium and solid aluminium–liquid cadmium surface energies as $\sigma_S - \sigma_L = 28$ and 25 mJ m^{-2}, i.e. in good agreement for the two different wheel speeds. The average difference can be taken as $\sigma_S - \sigma_L = 27$ mJ m^{-2}. Previous work has shown that σ_S of $\{1\,1\,1\}_{Al} \| \{0\,0\,0\,1\}_{Cd}$ facets is lower than the corresponding σ_L for melt-spun Al–4.5 wt % Cd, unlike the present observation of an average σ_S higher than σ_L. This difference can be attributed to the contribution of the curved interface regions surrounding the cadmium particles, as shown in Fig. 3.

Fig. 6 shows that the onset, peak and end temperatures of the cadmium particle solidification exotherms are independent of annealing temperature, i.e. are independent of cadmium particle melting temperature. This suggests that effect of the depression of cadmium particle equilibrium melting point on cadmium particle solidification exotherms is insignificant.

5. Conclusion

The melting points of 20 and 14 nm diameter cadmium particles embedded in an aluminium matrix in melt-spun Al–4.5 wt % Cd are depressed by 7 and 9 K, respectively, below the bulk equilibrium cadmium melting point, because of Gibbs–Thomson capillarity effects. The average solid cadmium particle/aluminium matrix interfacial energy is 27 mJ m^{-2} higher than the average liquid cadmium particle/aluminium matrix interfacial energy. No significant superheating is needed to nucleate cadmium particle melting.

Acknowledgements

We thank Professor Sir Peter Hirsch for provision of laboratory facilities, and Dr W. T. Kim for helpful

discussions. We also thank the UK Science and Engineering Research Council, the British Council and the State Education Commission of China for financial support of this research programme.

References

1. R. W. CAHN, *Nature* **323** (1986) 668.
2. *Idem, ibid.* **273** (1978) 491.
3. G. L. ALLEN, R. A. BAYLES, W. W. GILE and W. A. JESSER, *Thin Solid Films* **144** (1986) 297.
4. P. R. COUCHMAN and W. A. JESSER, *Nature* **269** (1977) 481.
5. V. P. KOVERDA, *Phys. Metal. Metall.* **51** (1981) 100.
6. S. J. PEPPIATT and J. R. SAMBLES, *Proc. R. Soc. Lond.* **A345** (1975) 387.
7. S. J. PEPPIATT, *ibid.* **A345** (1975) 401.
8. V. G. GRYANZOV, M. A. GURSKII, L. I. TRUSOV. and A. A. AIVAZOV, *Sov. Phys. Solid State* **24**(2) (1982) 297.
9. R. P. BERMAN and A. E. CURZON, *Canad. J. Phys.* **52** (1974) 923.
10. C. R. M. WRONSKI, *Br. J. Appl. Phys.* **18** (1967) 1731.
11. PH. BUFFAT and J-P. BOREL, *Phys. Rev. A* **13** (1976) 2287.
12. G. L. ALLEN, W. W. GILE and W. A. JESSER, *Acta Metall.* **28** (1980) 1695.
13. H. SAKA, Y. NISHIKAWA and T. IMURA, *Philos. Mag.* **A57** (1988) 895.
14. J. B. BOYCE and N. STUTZMANN, *Phys. Rev. Lett.* **54** (1985) 562.
15. C. J. ROSSOUW and S. E. DONNELLY, *ibid.* **55** (1985) 2960.
16. D. L. ZHANG and B. CANTOR, *Acta Metall. Mater.* **39** (1991) 1595.
17. D. L. ZHANG, K. CHATTOPADHYAY and B. CANTOR, *J. Mater. Sci.* **26** (1991) 1531.
18. T. B. MASSALSKI, J. L. MURRAY, L. H. MENNETT and H. BAKERS, in "Binary Alloy Phase Diagram" (American Society for Metals, OH, 1986).
19. W. T. KIM, D. L. ZHANG and B. CANTOR, *Met. Trans.* **22A** (1991) 2487.
20. "Metals Handbook", 9th Edn (American Society for Metals, OH, 1989).

Received 21 January
and accepted 21 September 1993